Wavefield separation in the presence of statics: application to synthetic and real data

Saul E. Guevara and Peter W. Cary

ABSTRACT

An algorithm for wave mode separation at a free surface, including the effect of statics, is applied to synthetic and real land data. The algorithm is based on the free surface response for vertical and horizontal geophones, which are expressed as a function of the horizontal slowness, *p*, and then are applied in the ω-*p* domain. Statics are introduced as a phase rotation in the frequency domain, and the data are inverted using a standard linear method, to obtain the P- and S- wave fields below the near-surface layer. Application to synthetic data confirms that the algorithm works well, but with some sensitivity to the near-surface velocity model. With real data there is no clear difference in prestack data, however there is some improvement of poststack data.

INTRODUCTION

P- and S-waves can be used together to increase the geological information that can be obtained about the subsurface. Thus a main goal in the multicomponent method is to obtain two independent seismic sections, one using P-wave and the other using S-wave data. In land surface seismic it is usual to assume that the vertical component records the data of P-waves and the horizontal component S-waves. However real data shows that this is not totally true, producing an effect known as “mode leakage”. Examples of this effect are shown by Lu et al, 1999 (this volume). Using a theoretical model of the land surface method, with the free surface boundary condition, it has been shown mathematically that, in two dimensions, two orthogonal components can detect both wave modes (e.g. Knopoff et al 1957, Evans, 1984). This is called the “free surface effect”. It depends on the type and incidence angle of the seismic event and on the near surface velocities.

Some methods have been proposed to separate wave modes. Dankbaar (1985) uses the free surface response equations in the f-k domain to perform the separation. Donati (1996) applies this method in the tau-p domain. This method has also been extended to marine data by Donati and Stewart (1996), which is currently a topic of great interest.

The land near-surface layer, usually heterogeneous and with low velocity, affects the seismic data. These characteristics produce relative delays in the arrival of the signal, and consequently there is distortion of the data from deeper layers. This shifting has to be compensated for in order to obtain a correct image of those layers, in a procedure known as “static correction”. With P-S data, all traces in a receiver gather are affected by the same large S-wave static, however the data are often aliased because of the large source separation, which is usually several times greater than the

receiver separation. Shot gathers are usually not aliased, however they are affected by S-wave receiver statics. A method is required which takes account of the statics problem whilst separating modes. An algorithm for mode separation which takes statics into account has been proposed by Cary (1998). It makes use of the free surface response and the horizontal variation in velocities of the near surface layer. Thus, in principle, this method can be applied advantageously to land data in the shot domain.

In this work the method proposed by Cary (1998) was applied to real and synthetic data and the results were analyzed. The method worked well with synthetic data and was robust with respect to errors in the near surface velocities. From the results on real prestack data and poststack sections, we believe that the method can improve velocity analysis and stacking, and hence can help to obtain better seismic sections.

DESCRIPTION OF THE ALGORITHM

The algorithm calculates the separated mode fields by applying generalized linear inversion to the input data (vertical and horizontal components) affected by statics and the free surface response. It works in the ω-p (frequency-horizontal slowness) domain.

The equations describing the free-surface effect are the result of solving wave propagation equations for incident plane waves with free-surface boundary conditions. These equations depend on the incidence angle and on the P- wave and S-wave velocities in the near surface. The free-surface response to unit incidence for two pairs of Vp and Vs velocities is illustrated in Figure 1. This Figure shows the amplitude variation in the vertical and horizontal directions as a function of the incidence angle of the wave. These curves show the coefficients that, when multiplied by the amplitude of the incident wave, allow the calculation of the resultant either in the vertical or horizontal direction. Subsequently the vertical and horizontal displacements can be defined as a “forward problem” represented by

$$D_V = R_{PV}\, U_P + R_{SV}\, U_S \qquad (1a)$$

$$D_H = R_{PH}\, U_P + R_{SH}\, U_S \qquad (1b)$$

where R_{PV} , R_{SV} , R_{PH} , R_{SH} are the coefficients of the free surface response (illustrated in Figure 1), U_P, U_S are the incident P- and S-wave fields, and D_V , D_H are the recorded vertical and horizontal data.

These equations can be defined in terms of the "ray parameter" or "apparent slowness", p. This parameter is used to describe plane waves, and is defined as

$$p = \frac{\sin\theta}{V}, \qquad (2a)$$

where θ is the incidence angle and V the wave velocity, or, equivalently,

$$p = \frac{\Delta t}{\Delta x}, \qquad (2b)$$

where, for a specific event, Δt is the time change corresponding to an space change Δx.

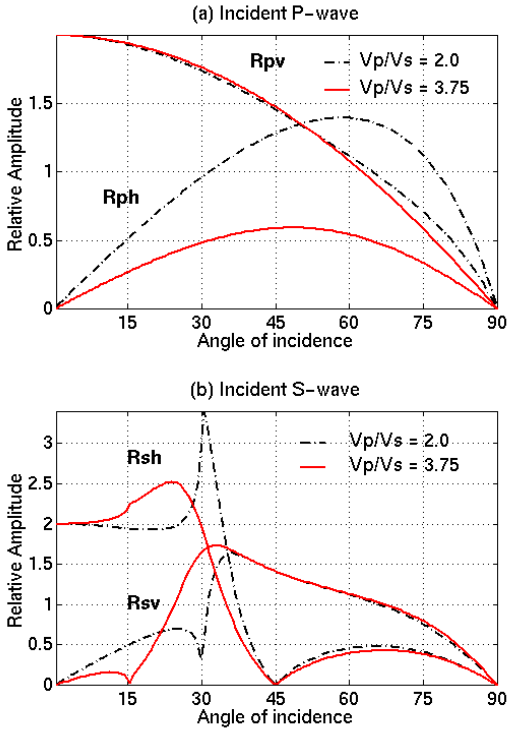

Figure 1. The free surface response.

The tau-*p* transform is a plane wave decomposition of the wave field (Stoffa et al, 1981) and the surface response equations can be written as a function of *p*. Therefore the equations 1a and 1b can be represented in the tau-*p* domain. The propagation of plane waves through the near-surface layer, interaction with the near-surface, and plane-wave synthesis (see Cary, 1998, for details) can be represented as

$$\mathbf{D} = \underline{\mathbf{B}}\,\mathbf{U} \qquad (3)$$

where **D** is a vector with the horizontal and vertical input data, $\underline{\mathbf{B}}$ is a matrix that contains the surface response and the static corrections in the ω-*p* domain, and **U** is a vector with the separated wavefields in the ω-*p* domain.

Thus the separated wavefields below the near-surface layer can be found applying the generalized linear inversion to equation (3),

$$\mathbf{U} = (\underline{\mathbf{B}}^{H} \underline{\mathbf{B}})^{-1} \underline{\mathbf{B}}^{H} \mathbf{D} \qquad (4)$$

This constitutes the basic procedure of the algorithm and is the more demanding in terms of computer time. The algorithm is described in the flow chart of Figure 2. It was coded in Matlab^{TM}.

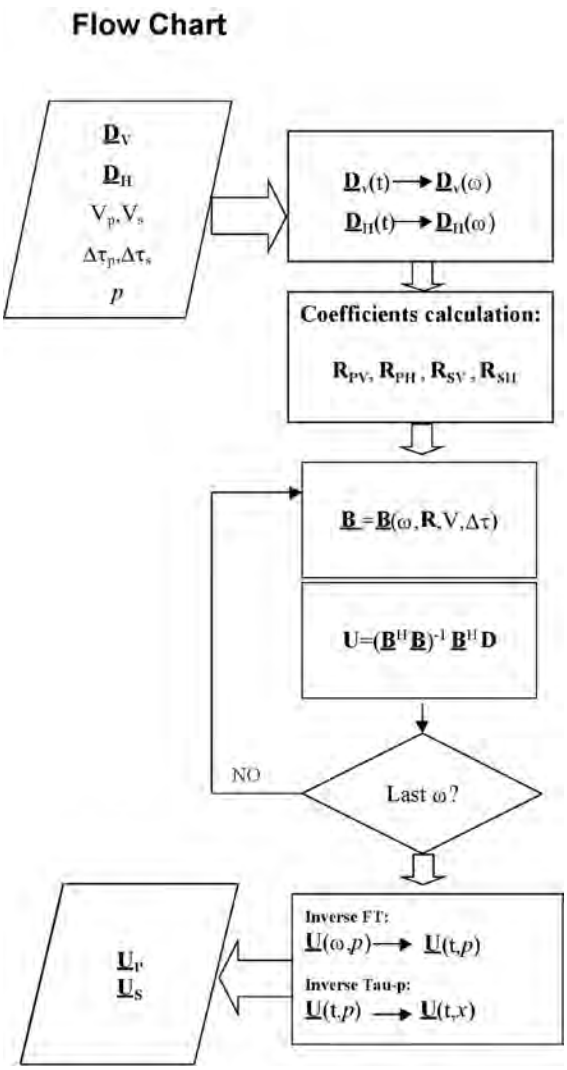

Figure 2. Flow diagram of the algorithm.

APPLICATION TO SYNTHETIC DATA

A simple geological model, used to test the method, is illustrated in Fig. 3. Fig. 4 shows the resulting synthetic vertical and horizontal components using a finite-difference method.

From analysis of velocities, polarization, and snapshots, the events labeled with numbers in Figure 4 are identified as:

(1) Direct wave, (2) Rayleigh wave, (3) P-wave reflection, (4) Converted wave reflections (P to S and S to P) and (5) S-wave reflection. The events (3), (4) and (5) are body waves, which are the target of mode separation in this work.

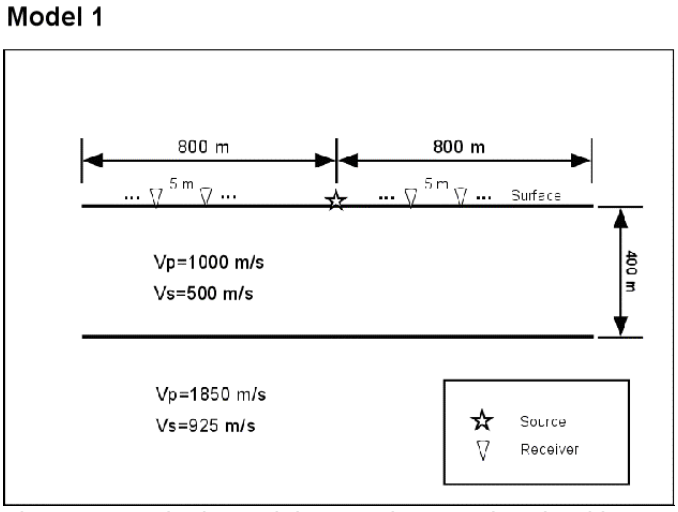

Figure 3. Geologic Model 1, used to test the algorithm.

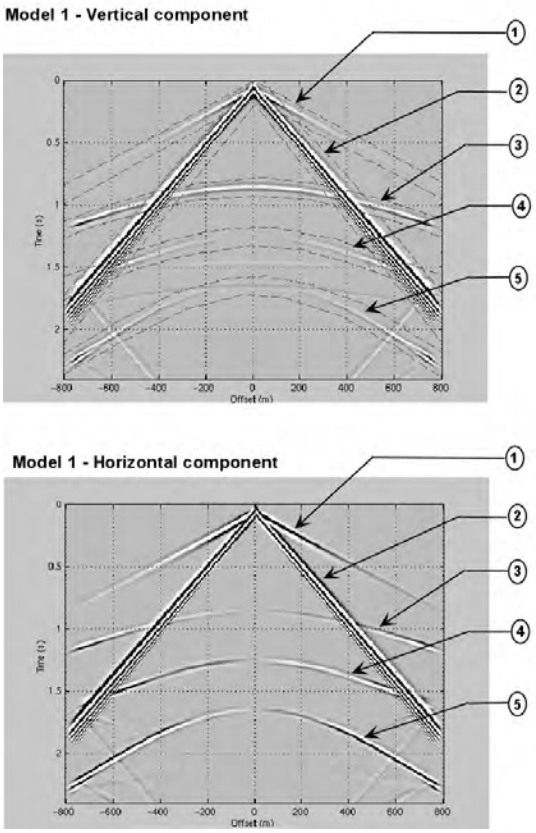

Figure 4. Resulting vertical and horizontal components for the model shown in Figure 1, using the FD method.

For convenience, only the right half of the spread was calculated and interfering effects of the near surface, like direct waves and ground roll, were eliminated. To this end, the synthetics were created using the Osiris^{TD} modeling software, which is based on the direct global matrix method. To simulate the statics effect, a simple time shift, which changes horizontally in three places was assumed. The data affected by the statics is illustrated in Fig. 5. The different static shifts for the P- and S- events on the same traces are indicated by the arrows. The near surface velocities were calculated from the statics, assuming a constant thickness of 20 m.

The results of the application of the method are shown in Figure 6. Figure 6a shows the P-wave field and Figure 6b the S-wave field. In the P wave field are the P-wave reflection and the S-to P- converted wave. In the S wave field are the P to S-converted wave and the pure S wave. These results agree with the analysis performed over the FD model referred above.

Exact values of the near-surface velocities are not easily available in multicomponent data. In order to test the effect of errors in near-surface velocities, a second example was used. Random statics were applied to Osiris data (wave-mode separated and then combined), as illustrated in Figure 7a. The velocities, Figure 7b, were calculated assuming a near-surface layer of 20 m. Input data to the algorithm are illustrated in Figure 7c and 7d. It is a very rough estimate of near-surface velocities. The average velocities were considered constant. The P-wave velocity is 850 m/s, and the S- wave velocity is 240 m/s. The results after the application of the method are shown in Figure 8. Although some mode "leakage" remains, the algorithm behaves reasonably well (compare with Figure 6.)

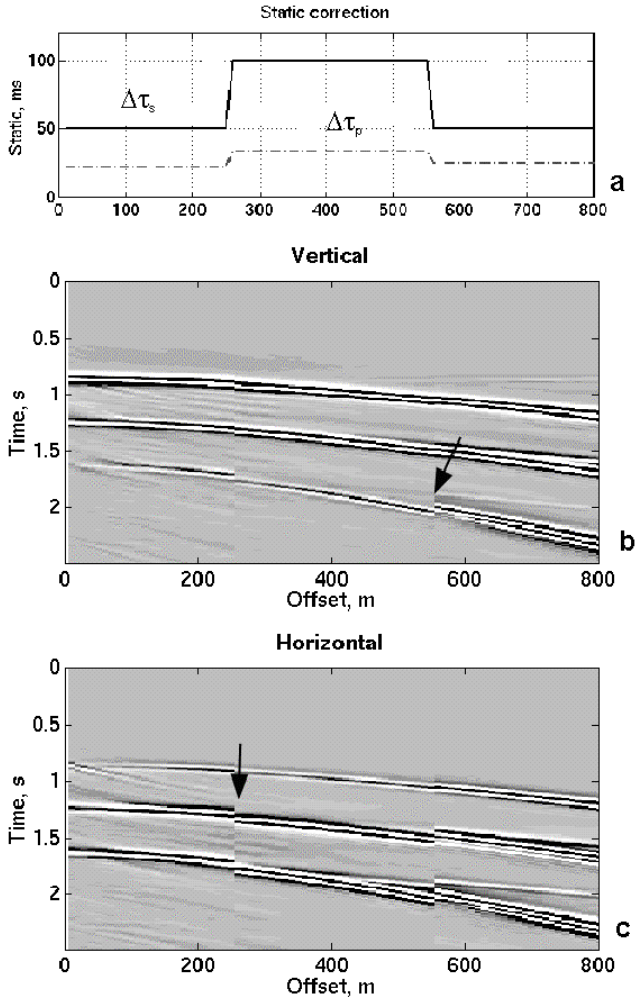

Figure 5. Model with simple statics delay applied.

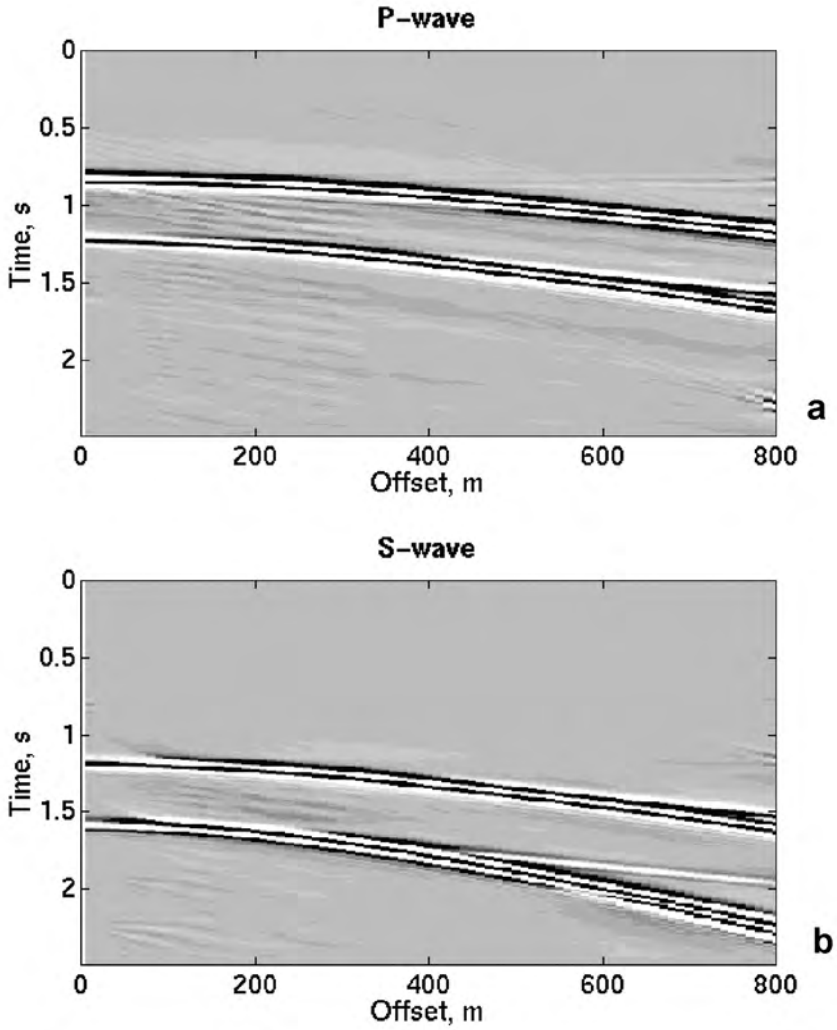

Figure 6.Result of separation of the simple statics model data.

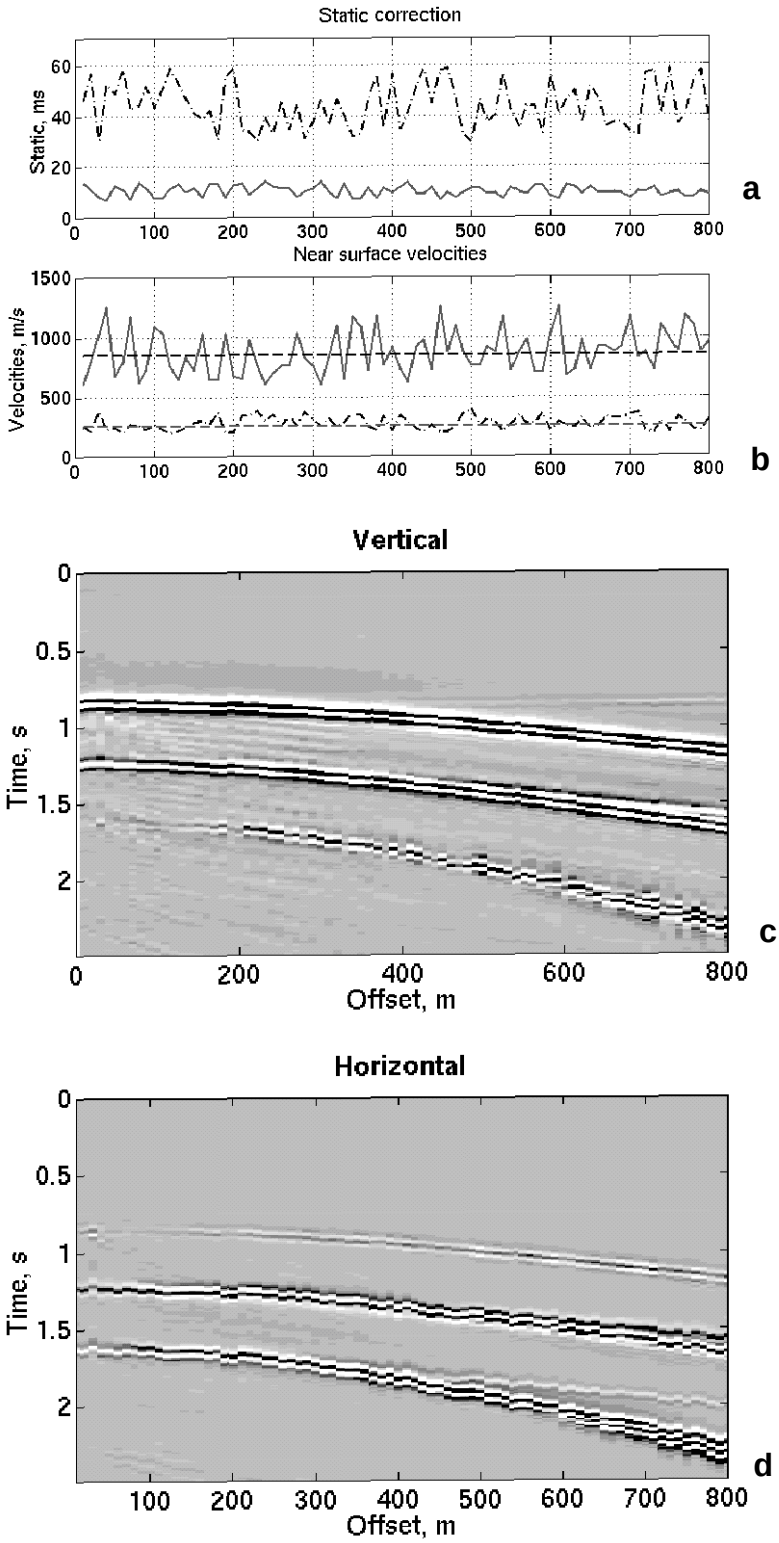

Figure 7. Model with random statics. (a) The statics corrections and (b) the velocity model. The horizontal lines show the velocity assumed. (c) is the vertical component, and (d) is the horizontal component.

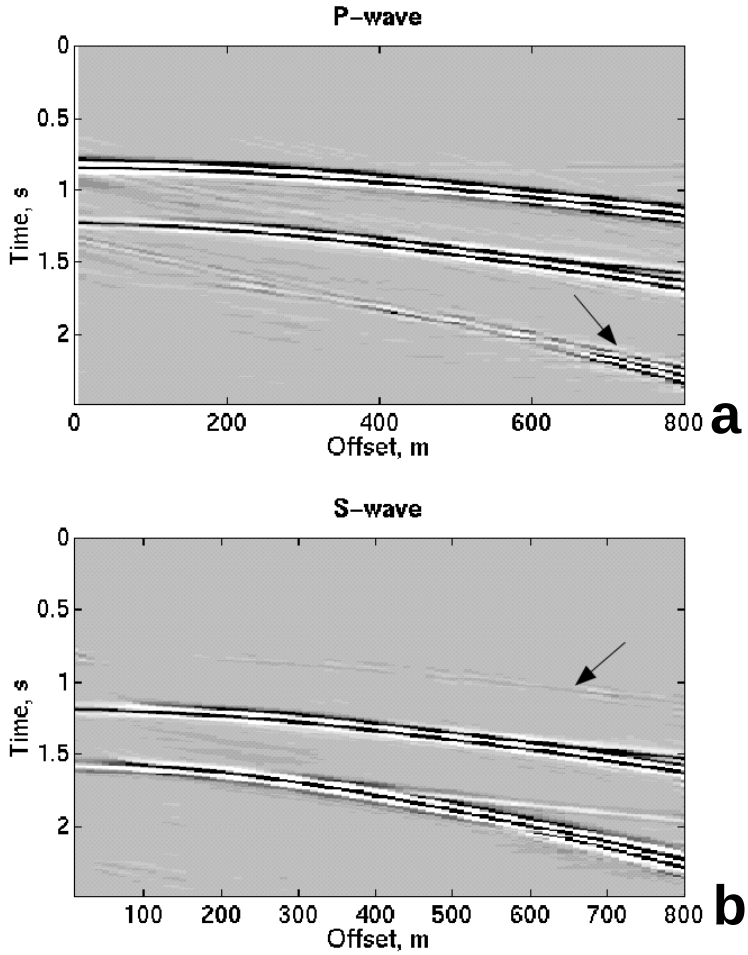

Figure 8. The data of figure 7 after separation. The arrows show remaining effects of mode leakage.

APPLICATION TO REAL DATA

The real data set

The method was applied to real data from the seismic survey Blackfoot III. This was an experimental 3C-2D seismic line acquired over an oil field belonging to Pan Canadian, 60 km SE of Calgary, Canada. It is a result of a research partnership between the industry and the CREWES project. A more complete description can be found in Hoffe et al, 1998.

The length of the line was 3 Km, with shots at 20 m intervals. A subset of the data, 29 shot separated by 100 m, were chosen to test the method. There were 151 receivers at 20 m intervals. Thus the spread is more typical of standard land multicomponent surveys, where the distance between sources is larger than the distance between receivers. The nominal charge depth was 18 m. The total record length was 2.5 s. To reduce the computational cost, the original data, with 1 ms sampling interval, was

resampled to 4 ms, hence there were 626 samples for each trace. The nominal fold for converted waves was reduced to 20, one fifth of the fold in the original data. As a previous step, the rotation of the data to get the optimum radial component was performed. An example of the raw data for the vertical and radial components is illustrated in Fig. 9.

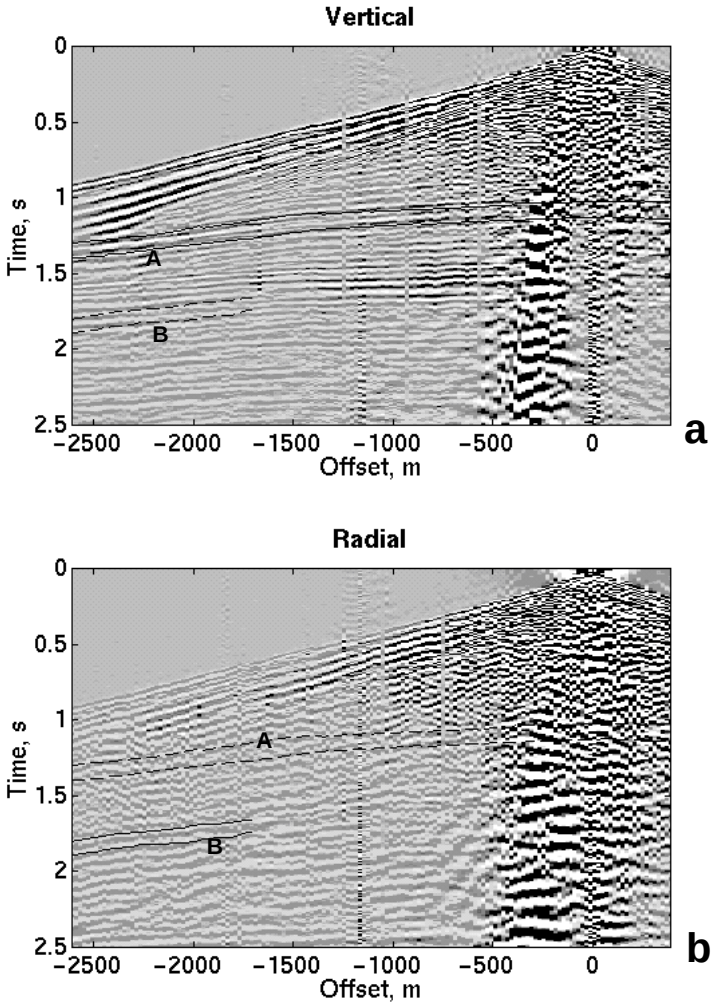

Figure 9. Shot gather of real data with (a) the vertical component and (b) the radial component.

Application to prestack data

Information and routines of a processing performed previously by CREWES (Lu et al, 1999) were used here. In order to calculate the near surface velocities, the receiver statics information was used, assuming a near surface layer of 20 m. The resulting velocities are shown in Fig. 10. Taking into account the uncertainties of the method, these velocities were compared with the results of two other sources of information: the near-surface work of Cieslewicz (1999) on the same line and the drilling information reported by the acquisition crew.

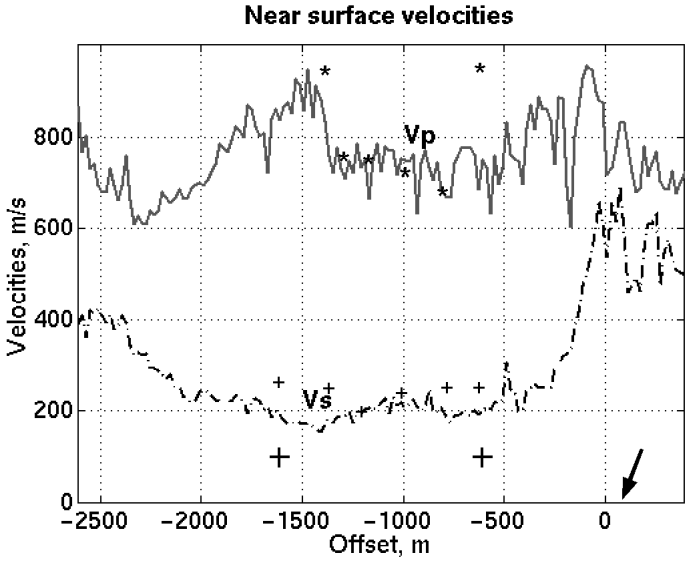

Figure 10. Near surface velocities for the Blackfoot III data.

Cieslewicz (1999) found the near surface velocities based on an experiment of buried geophones, which was part of the Blackfoot III survey. This experiment was carried out in the central kilometer of the same line studied here, using depths of 6, 12 and 18 m. The results for the 18 m geophones are shown with asterisks (V_p) and crosses (V_s) in Figure 10. A good agreement in the general trend with the data calculated here can be seen. From the records of the acquisition crew, sandstone was reported in the place shown with an arrow in Figure 10, probably an outcrop of quasi-intact rock. This event can explain the high near surface velocities found in that place, particularly for S-waves, and the high Vp/Vs ratio, more appropriate for consolidated rocks than for weathering layers. Hence, the velocities calculated correlate reasonably well with the information taken directly from the terrain.

The *p* values in the tau-*p* transform have a strong effect in the computational efficiency of the algorithm and in the potential creation of calculation artifacts. Hence the apparent slowness *p* has to be chosen using two criteria: sampling interval appropriate to control the aliasing effect (Turner, 1990) and a range of values that includes the events of interest. The window of data in Figure 9, was analyzed for its frequency content and its apparent slowness. The apparent slowness shows values between 33 and 45 ms/100 m. The maximum *p* value chosen was 50ms/100m.

According to Turner (1990), aliasing in the *p*-domain can be avoided choosing the sampling interval to be

$$\Delta p < \frac{1}{x_r f_{\max}} \qquad (5)$$

where x_r is the maximum offset, and $f_{\max}$ is the maximum frequency.

From the spectral analysis shown in Figure 11, 50 Hz can be considered the maximum frequency with information for the S event.

Substituing x_r = 3000 m

and f_{max} = 50 Hz in (5)

the sampling interval would be 0.666 ms/100 m

A value Δp = 0.5 ms/100 m = 5×10^{-6} s/m was chosen.

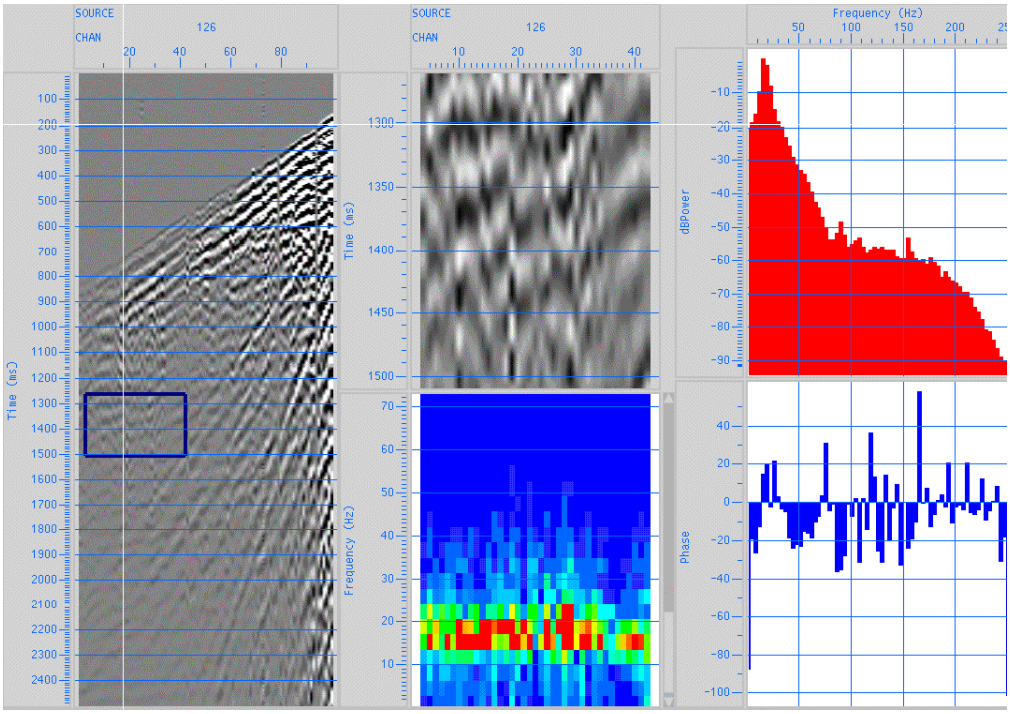

Figure 11. Spectral analysis for a window of the data in the Radial component.

The results of the application of the method to the same shot on Figure 9 are shown in Figure 12. In order to have information about the effect of mode separation, that is to say applying tau-*p* transform and statics only, the algorithm was applied without the effect of the conversion coefficients R. To do that, it were assumed constant coefficients

$$R_{PV} = R_{SH} = 1, \text{ and } R_{PH} = R_{SP} = 0.$$

The results are in Figure 13. Comparing Figures 12 and 13 it can be seen that the differences between the results are subtle, such it is difficult to evaluate the performance of the method in this way.

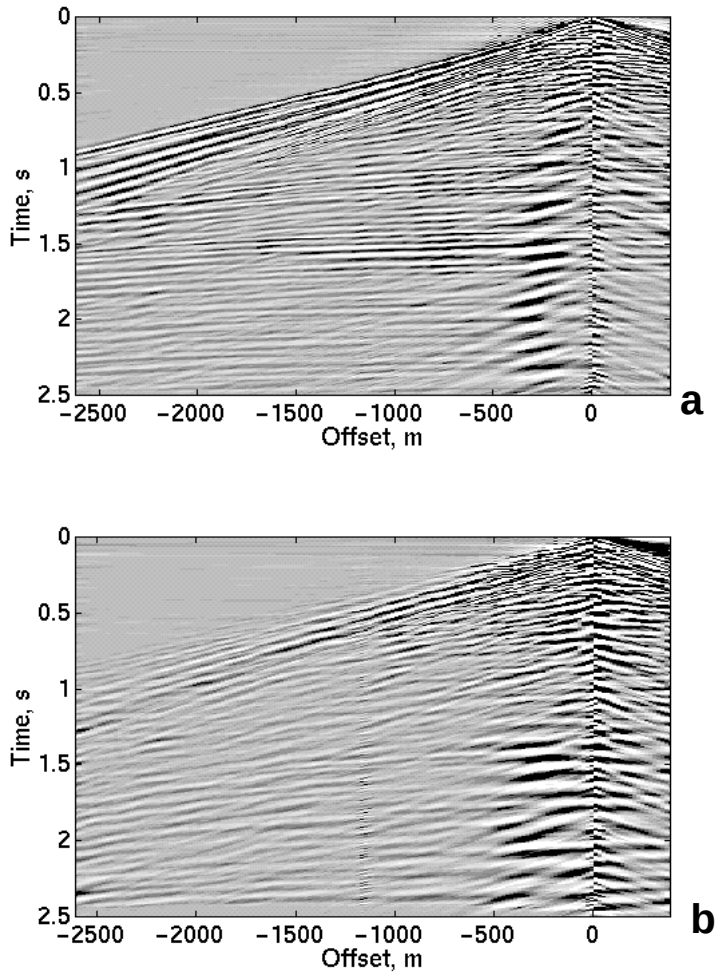

Figure 12. Result of the application of the algorithm of mode separation with statics to the real data (see Figure 9). (a) P-wave, (b) S-wave.

It can be noticed that the tau-*p* transform and statics have a filtering effect. This effect is related to the range of slowness chosen, such that the inverse tau-*p* transform can not reconstruct the events out of this range.

Besides the effect of noise in the data and of computational artifacts, the small size of the differences between Figure 12 and 13 can be explained with the help of theoretical free surface response. The curves of free surface response on Fig.1 correspond to velocities of the real data used here (see Fig.10.) The missing data are the incidence angles. In order to have an estimate of the incidence angle for representative events of the two wave modes, the plane wave approximation, equations (2), was applied. To this end two data windows were chosen, illustrated in Fig.9. The window 'A' corresponds to a P-wave event and the window 'B' to a S-wave. The resulting angles together with a linear approximation are shown in Fig. 14. For the farther offset the incidence angle would be 4 for P-wave and 9 for S-wave. Assuming these values and looking at the curves of free surface response (Fig. 1), the maximum amplitude in the horizontal component due to a P-wave could be 10% of

the vertical, and it would be the same or less for incident S-wave in relation with the vertical component.

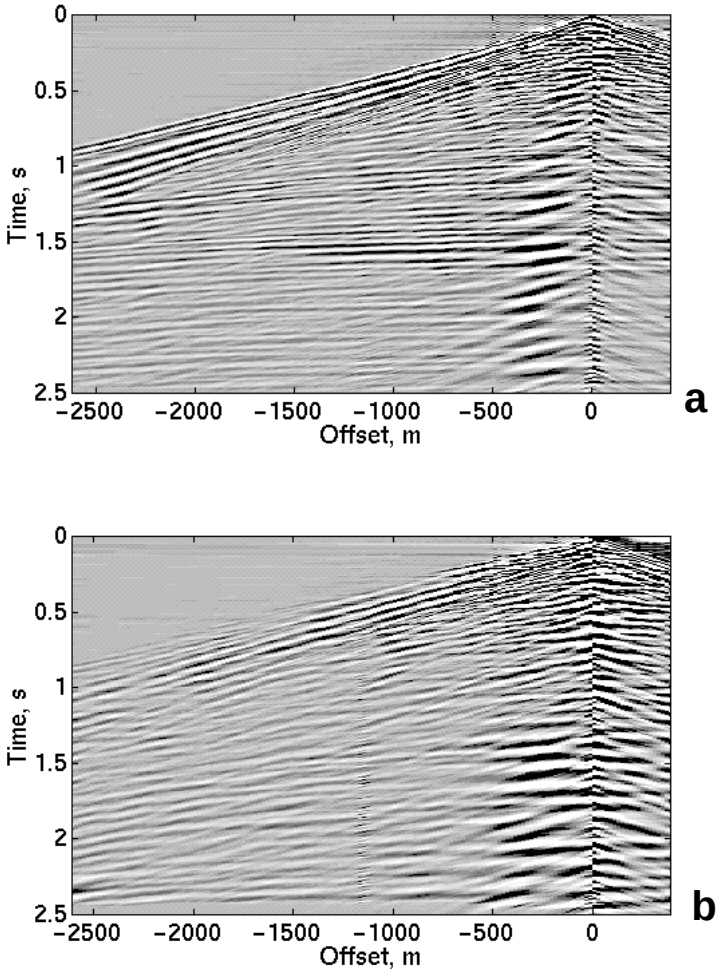

Figure 13. Result of the application of the algorithm without mode separation. (a) P-wave, (b) S-wave.

Hence the amplitude of the S- wave in the vertical component and the P-wave in the horizontal component would be less than 10% of the corresponding amplitudes of P-wave in the vertical component and S-wave in the horizontal.

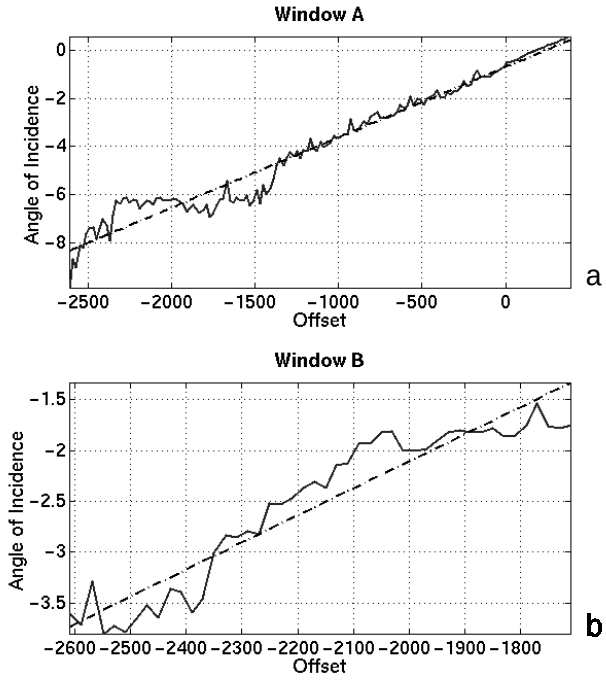

Figure 14: Angle of incidence according to the plane wave approximation for the windows of Figure 9 as a function of the offset. (a) angle from P-wave window and (b) angle from S-wave window. The dashed line is a linear approach.

Effect of mode separation on poststack data

The stacking process enhances the information content of seismic data. Since the prestack analysis is not very conclusive, we considered that poststack data could help in evaluating the performance of the algorithm.

Two stacked sections are compared, one without mode separation and the other one with mode separation. Each section results from the processing of the 29 shots. In order to get the data set without mode separation, the coefficients of the free surface effect are assumed one and zero, as described above. These coefficients have their true value to obtain the data set with mode separation.

The software ProMAX^{TM} was used for processing. A simple sequence was applied to the two datasets. This sequence, summarized in Figure 15 for S-wave, is a simplified version of the flow used at CREWES for research purposes (Lu et al, 1999). The nominal fold is around 20 (See Figure 16a).

The S-wave processing results are compared in Figures 16 and 17. Figure 17 is a close-up of Figure 16. Figures 16a and 17a show the result without mode separation and Figures 16b and 17b show the result with mode separation. Although the quality of the data is not homogeneous along the section, more continuity can be observed on some reflections after separation, as illustrated by the arrows in Figures 17a and 17b.

Processing Sequence for S-wave:

1. Input Filtered data SEG-Y.

2. Receiver statics substraction.

3. Surface consistent Deconvolution.

4. Asymptotic binning.

5. Rotation of rear component.

6. Application of elevation statics.

7. Application of Source and Receiver Refraction Statics, Hand statics and Residual statics.

8. NMO correction.

9. Time Variant Scaling.

10. Trace Muting.

11. Stack.

12. Poststack filtering.

Figure 15. Processing sequence for S-wave.

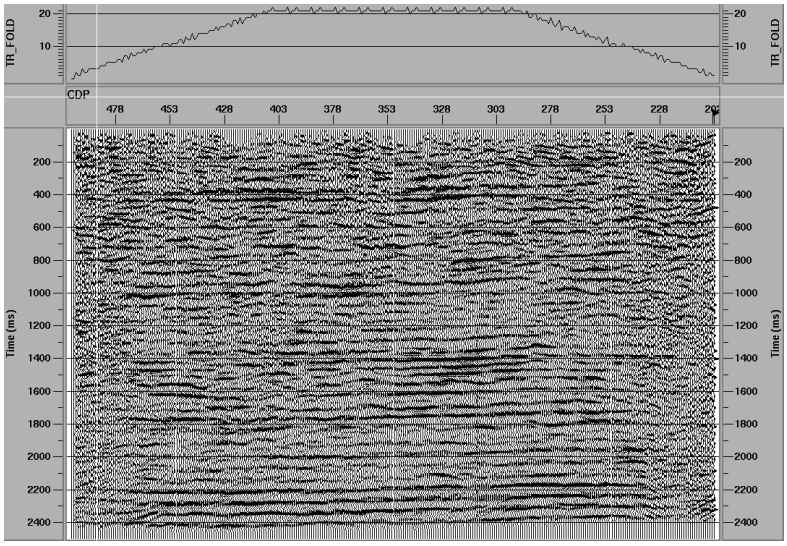

a

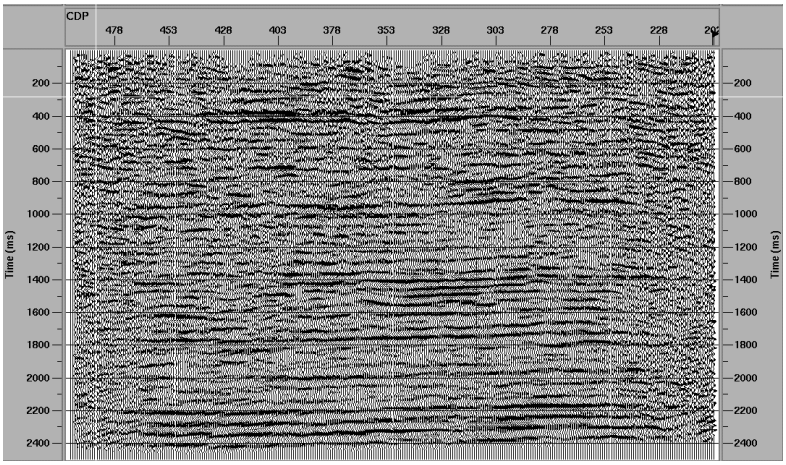

b

Figure 16: Processed seismic section of the S-wave after application of the algorithm. (a) without mode separation, and (b) with mode separation.

The processing parameters are not designed over this data set, and the result could change for a more specific processing flow, e.g. with a new velocity field.

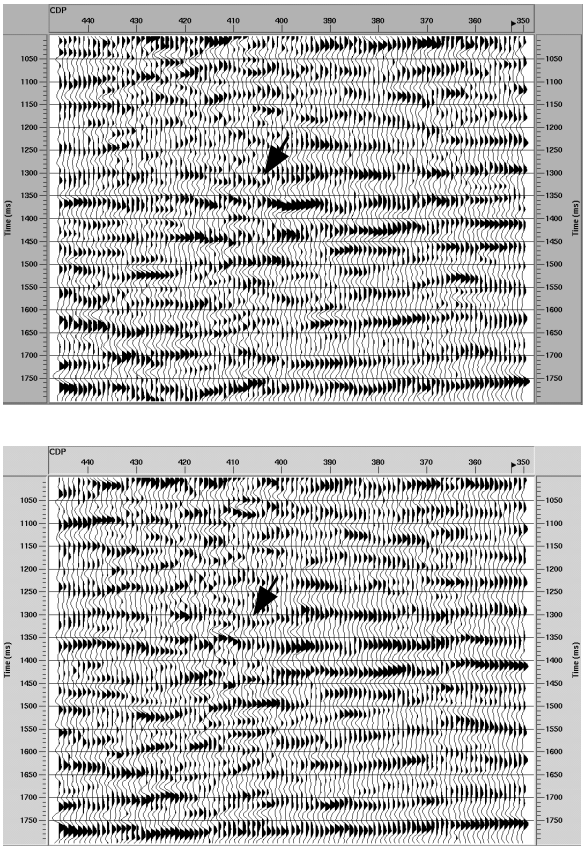

Figure 17. Close-up of Figure 16. (a) without mode separation, (b) with mode separation.

CONCLUSIONS AND FUTURE WORK

1. Tests performed show that the algorithm proposed by Cary (1998) works well for mode separation of synthetic data affected by statics.

2. The effect of mode separation is not so clear when the algorithm was applied to real data in the prestack domain. However, after the application of a simple processing flow, poststack data appear to have some increase in the information content because of the mode separation application.

3. The algorithm has additional filtering effects on the data, which can help to increase the information content.

4. The speed of computation is determined by the inversion step (Equation 4). Future work is needed to improve the efficiency of some of the steps in the inversion.

5. The relationship between mode separation and statics, illustrated by the method studied in this work, can be explored to help in the solution of two important problems associated with converted-wave data: increasing the information content of the P- and S-wave sections and improving the statics solution.

ACKNOWLEDGEMENTS

We thank Han-xing Lu for her support with data handling and processing, as well as the assistance of Henry Bland, Brian Hoffe, Xin-xian Li, Mary Emily Cargan and Graziella Kirtland Grech. Useful suggestions were given by Dr. Gary Margrave. The first author thanks the economic support of ECOPETROL.

REFERENCES

Cary, Peter W., 1998. P/S wavefield separation in the presence of statics. CREWES Research Report, Vol. 10., 30-1 to 30-8.

Cieslewitz, Dan, 1999. Near surface seismic characterization using three-component buried geophones. M. Sc. Thesis, Department of Geology and Geophysics, University of Calgary.

Dankbaar, J. W. M., 1985, Separation of P- and S-waves. Geophysical Prospecting 33, 970-986.

Donati, M. S., 1996, P- and S- wave separation using three component modal filters. M. Sc. Thesis, Department of Geology and Geophysics, University of Calgary.

Donati, M. S. and Stewart, R. R., 1996, P- and S-wave separation at a liquid-solid interface. Journal of seismic exploration 5, 113-127.

Evans, R., 1984, Effects of the free surface on shear wavetrains. Geophysical Journal of the Royal Astronomical Society 76, 165-172.

Hoffe, B., Stewart, R. R., Bland, H. C..,Gallant E. V. and Bertram, M., 1998, The Blackfoot high-resolution seismic survey: design and initial results. SEG 68th Annual Meeting, Expanded Abstracts, 103-106.

Knopoff, L., Fredrick, A. F., Gangi, A. F. and Porter, L. D., 1957, Surface amplitudes of reflected body waves. Geophysics, Vol. 22, No. 4, 842-847.

Lu, H-X. and Margrave. G. F., 1999, Study of the multiple mode conversion of the Blackfoot 3C seismic data. CREWES Research Report, Vol. 11.

Stoffa, P. L., Buhl, P., Diebold, J., and Wenzel, F., 1981, Direct mapping of seismic data to the domain of intercept time and ray parameter – A plane-wave decomposition. Geophysics, Vol. 46, No.3, 255-267.

Turner, G., 1990, Aliasing in the tau-*p* transform and the removal of spatially aliased coherent noise. Geophysics, Vol. 55, No. 11, 1496-1503.